ACS APPLIED MATERIALS & INTERFACES

Research Article

www.acsami.org

Facial Synthesis of PtM (M = Fe, Co, Cu, Ni) Bimetallic Alloy Nanosponges and Their Enhanced Catalysis for Oxygen Reduction Reaction

Zhijun Zhu,[†,‡] Yanling Zhai,[†,‡] and Shaojun Dong*[,†,‡]

[†]State Key Laboratory of Electroanalytical Chemistry, Changchun Institute of Applied Chemistry, Chinese Academy of Sciences, Changchun, Jilin 130022, China

[‡]University of Chinese Academy of Sciences, Beijing 100039, China

Supporting Information

ABSTRACT: Constructing electrocatalysts with enhanced activity and stability is necessary due to the increasing demands of the fuel cell industry. This work demonstrates a facile approach to synthesize well-defined three-dimensional (3D) PtM (M = Fe, Co, Cu, Ni) bimetallic alloy nanosponges (BANs) in the presence of Al. Significantly, with the aid of Al, the as-prepared BANs exhibit greatly enhanced electrochemistry catalytic activity in an oxygen reduction reaction (ORR), and PtFe BANs appear the best ORR property among the four BANs and commercial Pt/C catalysts. This work may provide a universal approach for convenient and large-scale fabrication of porous bimetallic nanocatalysts, thus providing promising potential application as an efficient cathodic component in fuel cells for industrial production.

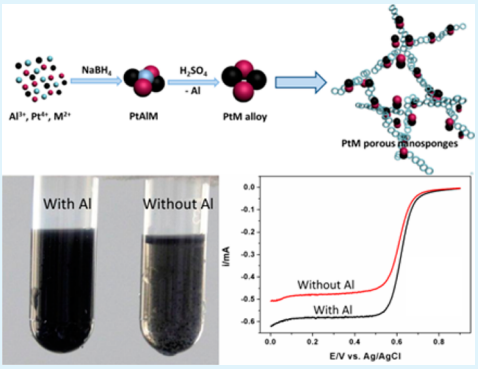

KEYWORDS: *facile method, Al-assistant, bimetallic alloy nanosponges, enhanced oxygen reduction reaction, high stability*

1. INTRODUCTION

Recently, fuel cells have been developed enormously because of their great potential application in modern life.[1] However, low current density and large overpotential existed in the current cathodic catalyst, limiting the industrial application of fuel cells.[2−5] Platinum has been studied extensively as an effective cathode material to reduce undesired overpotentials in the ORR due to its extraordinary electrocatalytic activities.[6,7] Due to the high costs, designing and exploring electrocatalysts with low-Pt content and enhanced catalytic activity and high stability are imperative for the industrialization of fuel cells. Pt-based alloy catalysts catch on due to less loading of the Pt and improved catalytic performance. Recently, various kinds of Pt-containing nanomaterials with enhanced ORR activity, such as PtAu,[8] PtPd,[9,10] PtAg,[11] and PtAuPd[12] have been explored. However, the noble metals, Pd, Ag, and Au were used in these works.

As key components for ORR, Pt-containing alloy nanostructures have attracted great interest. Early transition metals show enhanced synergistic catalytic effects to increase the catalytic performance of Pt catalysts and reduce the catalyst cost. Recently, great efforts have been made for the preparation of various PtM (M = Fe, Co, Cu, Ni, etc.) alloy nanomaterials and exploration of the alloying effect on the ORR activity of Pt.[13−15] Liu and co-workers fabricated graphene-supported PtCo nanostructures by reduction of mixed metal salts and studied their ORR catalytic activity in alkaline solutions.[16] Cindrella's group prepared a PtFeCo/carbon nanomaterials by a solvothermal method, also finding an enhancement for ORR activity.[17] Much attention has been paid to the preparation of PtM nanostructures with high ORR activities,[15,18−20] but these studies mainly involved complicated processes and employment of organic reagents. Therefore, the simple preparation of PtM alloy nanostructures with high catalytic performance is highly desired, because they show great potential application as an efficient catalyst in ORR.

As we know, composition and structure can greatly affect the performance of catalysts. A good catalyst should possess following features: (1) a high specific surface area; (2) fast electron transfer resulting from high conductivity; and (3) excellent stability of the structure and performance in practical application conditions. In this study, we present a general and facile approach to fabricate well-defined porous PtM alloy nanostructures in ethanol. The introduce of Al plays a crucial role in improving the ORR property of BANs, which can be totally removed after simple treatment.[21] Compared to the currently available Pt-based alloy nanomaterials for ORR, our strategy holds great promise in their synthesis and application. The benefits are as follows: (1) with the aid of Al, three-dimensional (3D) porous BANs without any modifier/surfactant can be

Received: June 12, 2014
Accepted: September 16, 2014
Published: September 16, 2014

Scheme 1. Preparation of PtM Porous Nanosponges

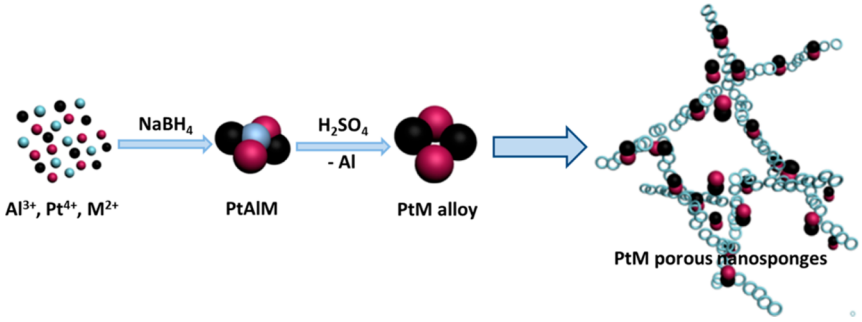

synthesized conveniently; (2) 3D porous BANs exhibit good dispersion, greatly enhanced electrocatalytic activity, and excellent stability, and PtFe BANs exhibit the best ORR activity; and (3) convenient and large-scale fabrication leads to the potential for industrial production, providing promising potential application as an efficient cathodic component in fuel cells.

2. EXPERIMENTAL SECTION

2.1. Materials. H_2PtCl_6 was obtained from Shanghai Chemical Reagent Co., Ltd. (Shanghai). $NaBH_4$ was obtained from Sigma-Aldrich. Commercial Pt/C (20% Pt mass loading) catalyst was obtained from Alfa Aesar. $Co(NO_3)_2$, $FeCl_2$, $CuCl_2$, $Ni(NO_3)_2$, $Al(NO_3)_3$, ethanol (99.9%), and other reagents were obtained in analytical grade.

2.2. Apparatus. The elementary analysis was performed on 6300 ICP equipment (Thermo Scientific, Waltham, MA). Transmission electron microscopy (TEM) measurements were performed on a Hitachi H-600 microscope (Japan, 100 kV), and JEM-2010 microscope (Japan, 200 kV) for high-resolution TEM (HRTEM). Scanning electron microscope (SEM) characterizations were carried on a Philips-FEI (XL-30, Netherlands). X-ray diffraction (XRD) experiments were carried on a D8 Advance Powder Diffractometer (Bruker, Ettlingen, Germany). Electrochemical experiments were carried on a CHI 832C electrochemical analyzer (Chenhua, Shanghai). BAS rotating ring/disk electrode (Japan) was used in electrochemical measurements. Ag/AgCl (KCl saturated) was used as a reference electrode and platinum wire was used as a counter electrode.

2.3. Synthesis of PtM (M = Cu, Ni, Co, Fe) Nanosponges. H_2PtCl_6, $Co(NO_3)_2$, $FeCl_2$, $CuCl_2$, $Ni(NO_3)_2$, and $Al(NO_3)_3$ were separately dissolved into ethanol to reach a final concentration of 0.1 M. Then, 200 μL of H_2PtCl_6, 200 (or 67, 33.5) μL of $FeCl_2$ (or $Co(NO_3)_2$, $CuCl_2$, $Ni(NO_3)_2$), and 400 μL of $Al(NO_3)_3$ were added into 3 mL of ethanol under continuous stirring at room temperature. Afterward, 10 mg of $NaBH_4$ dispersed in 2 mL of ethanol was injected into the above solutions under stirring, and color of solutions changed from light yellow to darkish. After stirring for 5 min, the mixtures were then centrifuged. Then, the as-prepared PtM BANs were washed with H_2SO_4 (0.5 M, 4 mL) under slight sonication to remove Al and Fe in PtM BANs. The product without Al added during synthesis procedure was used as control (denoted as PtFe1).

2.4. Electrocatalytic Experiment. The acid-treated PtM BANs were dispersed in a mixed solution of water, Nafion, and isopropyl alcohol, and the mixture was ultrasonicated to obtain a 2 mg/mL well-dispersed suspension. The glassy carbon (GC) rotating disk electrode (0.196 cm^2) was used as the working electrode. The GC electrode was polished carefully with 0.3 and 0.05 μm α-Al_2O_3 powder successively before surface coating. Then, the electrode was washed with water and ethanol, and dried under N_2 flow. Afterward, 10 μL of the prepared suspension was dropped onto the GC disk. After drying, the catalyst film modified GC was obtained. The commercial Pt/C (20 wt %) suspension was prepared following the same procedure as described above. The test solution was 0.5 M H_2SO_4. The catalysts were first scanned in the N_2-saturated solution with a scanning rate of 50 mV s^{-1} to obtain stable cyclic voltammogram. The ORR polarization curves were obtained in 0.5 M H_2SO_4 solution (O_2-saturated) with a scanning

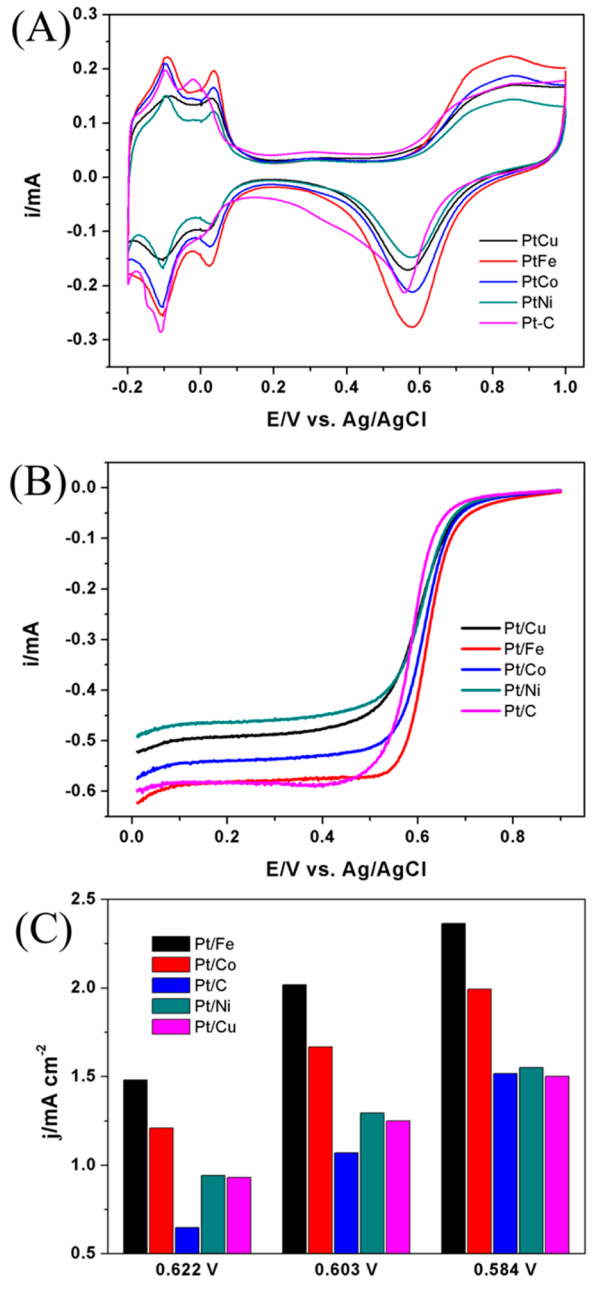

Figure 1. (A) CVs and (B) polarization curves of as-prepared PtM (M = Fe, Co, Ni or Cu) BANs and Pt/C catalysts in 0.5 M H_2SO_4 saturated with (A) N_2 and (B) O_2. (C) ORR activities of five catalysts at 0.584, 0.603, and 0.622 V.

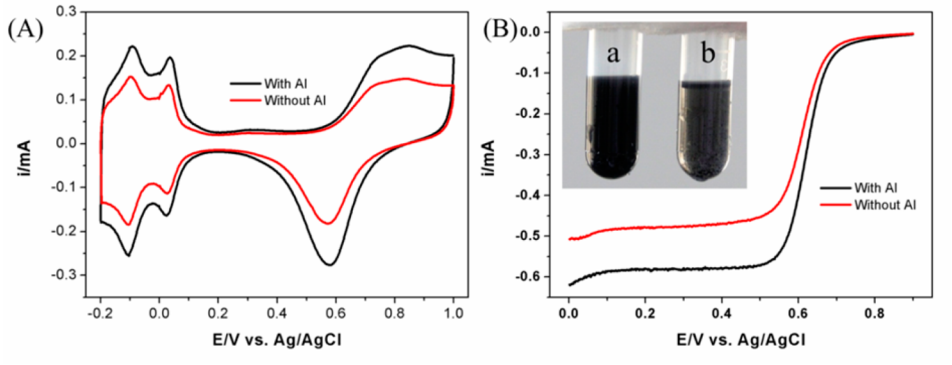

Figure 2. (A) CVs and (B) polarization curves of the PtFe BANs with or without Al used in the synthesis reaction in O_2 saturated 0.5 M H_2SO_4; (inset) photograph of the reaction mixtures in the (a) presence or (b) absence of Al.

rate of 10 mV s^{-1} at 1600 rpm. The stability test was performed by potential sweeping between 0.4 and 0.8 V in 0.5 M H_2SO_4 solution (O_2-saturated) at a scanning rate of 100 mV s^{-1}.

3. RESULTS AND DISCUSSION

3.1. Electrocatalytic Activities of Porous PtM (M = Fe, Cu, Co and Ni) Nanostructures. Our strategy for the fabrication of porous Pt-based BANs is outlined in Scheme 1. In the first step, a ethanal solution of $NaBH_4$ was quickly injected into ethanol solution containing H_2PtCl_6, $Al(NO_3)_3$, $Co(NO_3)_2$, or $FeCl_2$, or $CuCl_2$, or $Ni(NO_3)_2$, respectively, under stirring at room temperature. After stirring for about 5 min, the solution color turned from light yellow to black. The PtM BANs were obtained after being washed with H_2SO_4 under slight sonication to remove Al and excess Fe. The morphology and structure of the as-prepared PtFe BANs (with Pt/Fe precursors ratio = 3:1) were measured by using SEM and TEM. As shown in Figure S1 (Supporting Information), a sponge-like structure with porous and interconnected networks was fabricated on a large scale, which is favorable to spread and diffuse electrolyte ions.[22] Meanwhile, porous PtCo, PtNi, and PtCu BANs with homologous structures have also been obtained (data not shown), suggesting this protocol may provide an efficient method for facile synthesis of porous BANs. Next, we compared the electrocatalytic activity of these four alloy nanostructures to obtain the optimized electrocatalyst. Figure 1A reveals the cyclic votammograms (CVs) of the PtM nanostructures with sweep rate of 50 mV s^{-1} in 0.5 M H_2SO_4 (saturated with N_2). The peak in the potential of −0.2 to 0.1 V should be due to the adsorption and desorption of hydrogen, and the potential range of 0.4−0.8 V is ascribed to metal oxidation−reduction. In negative sweep, the peaks at around 0.57−0.58 and 0.558 V should be attributable to the reduction of Pt oxide in PtM BANs and commercial Pt/C, respectively. Among the four BANs, PtFe presents the most positive reduction potential, which is much better than that of commercial Pt/C. In addition, the obtained PtFe BANs exhibit greater electrochemically active surface area, which is beneficial to the enhanced electrocatalytic activity of catalysts. The ORR electrocatalytic activity was tested in 0.1 M H_2SO_4 solution saturated with O_2. The polarization curves of PtM nanostructure and commercial Pt/C catalyst are shown in Figure 1B. The potential between 0.5 and 0.7 V is ascribed to the mixed kinetic−diffusion control process, and the potential from 0.1 to 0.4 V is assigned to the diffusion limiting current.[18] As expected, the PtFe nanostructures exhibited the highest activity for ORR, which corresponds to the CVs shown in Figure 1A. The half wave potential (Figure 1B) of PtFe (0.622 V) is a bit higher than that of PtCo (0.615 V), PtCu (0.603 V), and PtNi (0.609 V), and much higher than that of commercial C/Pt (0.584 V), demonstrating that the PtFe BANs have the highest ORR electrocatalytic activity (Figure 1C). The excellent ORR activity of PtFe BANs might be attributed to the enhancement of the catalytic activity of Pt due to the downshift of Pt d-band electron structure after alloyed with Fe.[21]

Furthermore, the crucial role of Al in the BANs formation and performance was investigated in detail. It can be clearly found that the obtained PtFe alloy without Al addition in the procedure emerged obvious aggregation (Figure 2B, inset), and the structure was composed of larger building blocks (Figure S2, Supporting Information), which is not favorable for electrocatalytic activity. Their corresponding ORR catalytic activity was then studied together. Evidently, the synthesized PtFe BANs in the presence of Al showed higher electrochemically active surface area (Figure 2A), positive initial reduction potential and significant increase in diffusion-limiting current for ORR (Figure 2B). Therefore, the introduction of Al in our strategy plays a critical role in improving the catalytic property of BANs.

3.2. Characterization and Electroactivity of PtFe BANs with Different Pt/Fe Ratios. The composition ratio in BANs can be easily altered by changing the ratio of metal precursors. As a comparison, we will optimize the mole ratio between Pt and M and further obtain the PtM BANs with the best electrochemical performance. Taking PtFe BANs as an example, when the ratios of Pt and Fe were set to be 1:1, 3:1, and 6:1 in the precursors, $Pt_{53}Fe_{47}$, $Pt_{76}Fe_{24}$, and $Pt_{86}Fe_{14}$ were obtained through ICP-AES analyses. However, after washing with H_2SO_4, partial Fe in PtFe was lost, and $Pt_{79}Fe_{21}$, $Pt_{81}Fe_{19}$ and $Pt_{86}Fe_{14}$ were finally obtained, which has also been observed in previous work.[18] It should be noted that unlike others, the PtFe BANs with Pt/Fe ratio 6:1 in reaction mixture remained almost unchanged before and after being washed with H_2SO_4, which may be because it tends to form Pt_3M_1 nanostructures.[23,24]

The structural profile of the as-prepared $Pt_{79}Fe_{21}$ alloy was further characterized by typical SEM and TEM (Figure 3A,B). It is observed that porous alloy nanostructures are composed of about 4 nm nanoparticles. The inset of Figure 3B shows the single-crystalline structure of the PtFe alloy. The interplanar spacing of the lattice fringes was measured to be 2.2 Å, corresponding to the (111) crystal face of PtFe alloy nanocrystals.[22,25] Figure 3C−E shows the high-angle annular dark-field scanning TEM image of as-prepared $Pt_{79}Fe_{21}$ BANs and

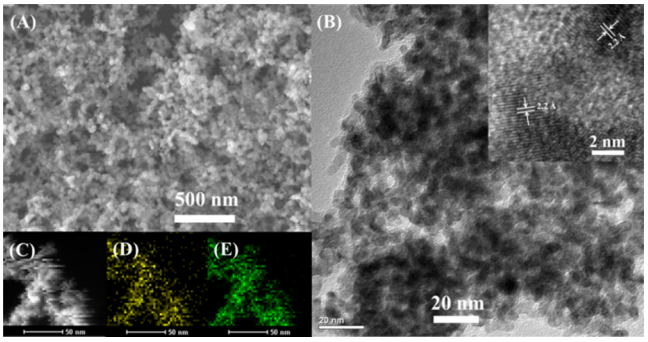

Figure 3. (A)TEM, (B) SEM, and (B, inset) HRTEM images of the as-obtained $Pt_{79}Fe_{21}$ BANs. HAADF-STEM-EDS mapping images of (C) $Pt_{79}Fe_{21}$ BANs, (D) Fe-L, and (E) Pt-L.

the related mapping with Fe-L and Pt-L. The corresponding element distribution in the same place demonstrated the formation of the alloy nanocrystals.

Figure 4 shows the wide-angle XRD pattern of the as prepared $Pt_{79}Fe_{21}$ BANs. The broadening of diffraction peak around

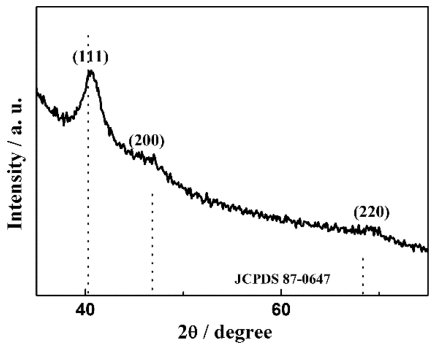

Figure 4. XRD pattern of $Pt_{79}Fe_{21}$ BANs.

40° is ascribed to the (111) planes of Pt. The other two characteristic diffraction peaks located at 46.2° and 68.0° correspond to the (200) and (220) planes (JCPDS 87-0647), respectively.[22] The peak of PtFe nanomaterial is located between that of Pt and Fe, suggesting formation of Pt−Fe alloy nanostructures.[22]

Furthermore, we compared the electrocatalytic activity of these three PtFe BANs. Figure 5 shows the typical CV curves of $Pt_{79}Fe_{21}$, $Pt_{81}Fe_{19}$, and $Pt_{86}Fe_{14}$ BANs in 0.5 M H_2SO_4 (N_2-saturated) at a sweep rate of 50 mV s^{-1}. It can be clearly found that $Pt_{79}Fe_{21}$ showed larger double-layer capacitance than $Pt_{81}Fe_{19}$. Figure 5A illustrates the ORR polarization curves of $Pt_{79}Fe_{21}$, $Pt_{81}Fe_{19}$, and $Pt_{86}Fe_{14}$ BANs in O_2-saturated 0.5 M H_2SO_4. We can see that the $Pt_{79}Fe_{21}$ BANs possess more positive half-wave potential (0.631 V) compared with that of the $Pt_{81}Fe_{19}$ BANs (0.622 V) under the same conditions. However, the $Pt_{86}Fe_{14}$ BANs have a negative half-wave potential (0.618 V), which indicates $Pt_{86}Fe_{14}$ BANs have smaller active area. The $Pt_{79}Fe_{21}$ BANs have an ORR activity about 2 times higher than that of the commercial Pt/C, between 0.584 and 0.622 V (Figures 5B and 1C). Moreover, compared with commercial Pt/C catalyst, the half-wave potential of $Pt_{79}Fe_{21}$ BANs negatively shifted about 50 mV (Figure 1B).

In addition to high activity, excellent stability is also crucial in fuel cells. The stability of $Pt_{79}Fe_{21}$ was tested with potential sweeps. Durability tests were carried by cyclic scanning between 0.4 and 0.8 V (100 mV/s) in 0.5 M H_2SO_4 (saturated with O_2).[18] As shown in Figure 6A, after 8000 potential sweeps, only

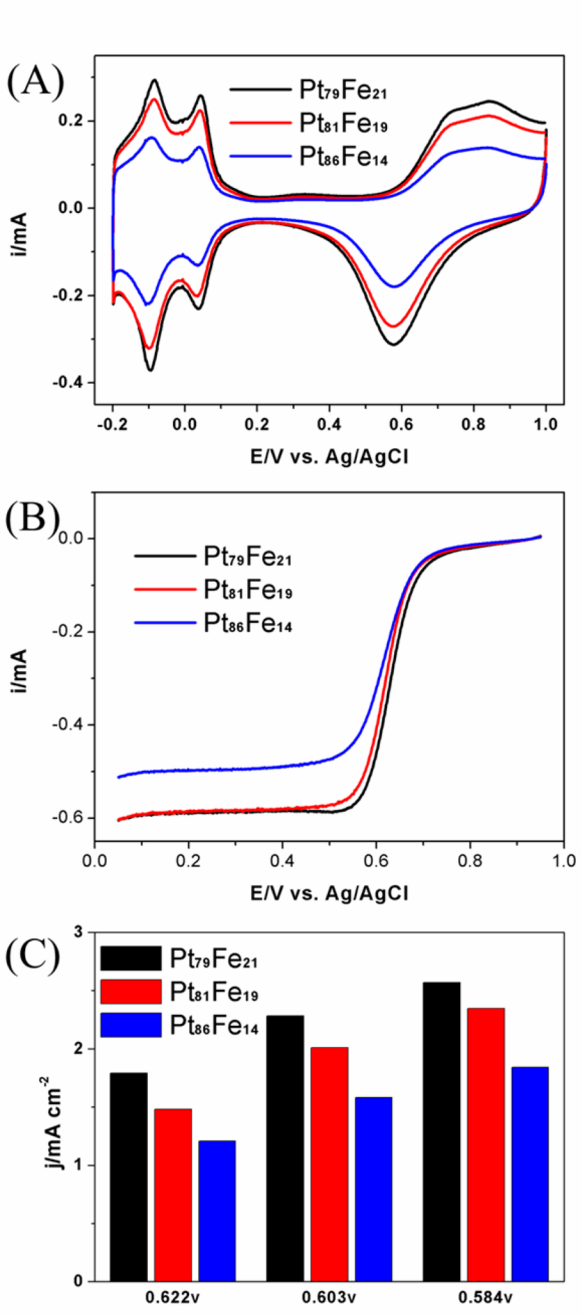

Figure 5. (A) CVs and (B) polarization curves of the $Pt_{79}Fe_{21}$, $Pt_{81}Fe_{19}$, and $Pt_{86}Fe_{14}$ BANs in O_2-saturated 0.5 M H_2SO_4. (C) ORR activities of the five catalysts at 0.584, 0.603, and 0.622 V.

2% decreases in the electrochemically active surface area. The polarization curves of the $Pt_{79}Fe_{21}$ after 2000 and 8000 potential sweeps are shown in Figure 6B. We can see that the $Pt_{79}Fe_{21}$ preserved almost all of the initial activity after these potential cycles, with only slight changes of the ORR polarization curves before and after the stability test. As a comparison, the $Pt_{81}Fe_{19}$ BANs are not so stable after even 2000 potential sweeps, and ORR polarization curve shifted obviously than before (Figure S3, Supporting Information). This demonstrates that $Pt_{79}Fe_{21}$ BANs are more suitable as a stable catalyst for ORR than others. Three main factors may account for the superior ORR activity and excellent stability of $Pt_{79}Fe_{21}$ BANs: (1) the Pt electron structure of d-band center downshifted after

dx.doi.org/10.1021/am503689t | ACS Appl. Mater. Interfaces 2014, 6, 16721−16726

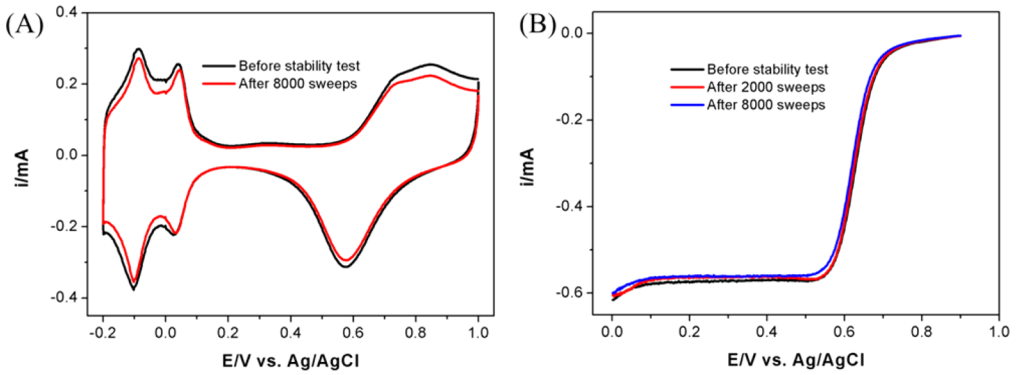

Figure 6. (A) CVs and (B) polarization curves of the $Pt_{79}Fe_{21}$ BANs before and after 8000 sweeps between 0.4 and 0.8 V.

alloyed modification with Fe;[21] (2) the mole ratio of Pt/Fe (79:21) reaches the most steady structure; and (3) the BANs with pore structures allow for easy permeation of the electrolyte and oxidant, and support fuel transport to the catalyst reaction sites thus generate enhanced current and long-time stability.

4. CONCLUSIONS

In summary, we have provided a new and universal approach for the preparation of unique PtM (M = Fe, Co, Ni, Cu) BANs with porous structure. The Al was crucial for the synthesis of the 3D porous PtM nanostructures. Different components and mole ratios were fully optimized for the preparation of catalysts with the highest performance. The porous $Pt_{79}Fe_{21}$ BANs were demonstrated as an effective catalyst with improved performance and excellent durability in ORR, which could be due to the high specific surface area and the porous structure as a result of the 3D structures. This indicates that catalysts with excellent performance can be produced by engineering the component and structure of the nanomaterials. This work not only offers a general method for convenient and large-scale fabrication of porous metallic nanocatalysts, but it also provides an approach to fabricate high performance porous catalysts with great practical potential in fields of the catalysis, energy, and sensors.

■ ASSOCIATED CONTENT

Supporting Information

SEM and TEM images of PtFe BANs, SEM image of PtFe1 BANs, CVs and polarization curves of $Pt_{81}Fe_{19}$ before and after stability test. This material is available free of charge via the Internet at http://pubs.acs.org.

■ AUTHOR INFORMATION

Corresponding Author

*Tel: +86-431-85262101. Fax: +86-431-85689711. E-mail: dongsj@ciac.ac.cn.

Author Contributions

Z. Zhu and Y. Zhai contributed equally to this work.

Notes

The authors declare no competing financial interest.

■ ACKNOWLEDGMENTS

This work was supported by 973 Project (Nos. 2011CB911002 and 2010CB933603) and the National Natural Science Foundation of China (No 21375123).

■ REFERENCES

(1) Yin, H.; Tang, H.; Wang, D.; Gao, Y.; Tang, Z. Facile Synthesis of Surfactant-Free Au Cluster/Graphene Hybrids for High-Performance Oxygen Reduction Reaction. *ACS Nano* **2012**, *6* (9), 8288−8297.

(2) Zhu, C.; Dong, S. Recent Progress in Graphene-based Nanomaterials as Advanced Electrocatalysts toward Oxygen Reduction Reaction. *Nanoscale* **2013**, *5* (5), 1753−1767.

(3) Bing, Y.; Liu, H.; Zhang, L.; Ghosh, D.; Zhang, J. Nanostructured Pt-Alloy Electrocatalysts for PEM Fuel Cell Oxygen Reduction Reaction. *Chem. Soc. Rev.* **2010**, *39* (6), 2184−2202.

(4) Zhai, Y.; Zhu, C.; Wang, E.; Dong, S. Energetic Carbon-based Hybrids: Green and Facile Synthesis from Soy Milk and Extraordinary Electrocatalytic Activity toward ORR. *Nanoscale* **2014**, *6* (5), 2964−2970.

(5) Wang, S.; Yu, D.; Dai, L.; Chang, D. W.; Baek, J.-B. Polyelectrolyte-Functionalized Graphene as Metal-Free Electrocatalysts for Oxygen Reduction. *ACS Nano* **2011**, *5* (8), 6202−6209.

(6) Ghosh, S.; Sahu, R. K.; Raj, C. R. Shape-Regulated High-Yield Synthesis of Electrocatalytically Active Branched Pt Nanostructures for Oxygen Reduction and Methanol Oxidation Reactions. *J. Mater. Chem.* **2011**, *21* (32), 11973−11980.

(7) Wang, C.; Daimon, H.; Lee, Y.; Kim, J.; Sun, S. Synthesis of Monodisperse Pt Nanocubes and Their Enhanced Catalysis for Oxygen Reduction. *J. Am. Chem. Soc.* **2007**, *129* (22), 6974−6975.

(8) Iijima, Y.; Kondo, T.; Takahashi, Y.; Bando, Y.; Todoroki, N.; Wadayama, T. Oxygen Reduction Reaction Activities for Pt/Au(*hkl*) Bimetallic Surfaces Prepared by Molecular Beam Epitaxy. *J. Electrochem. Soc.* **2013**, *160* (8), F898−F904.

(9) Fu, G.; Wu, K.; Lin, J.; Tang, Y.; Chen, Y.; Zhou, Y.; Lu, T. One-Pot Water-Based Synthesis of Pt−Pd Alloy Nanoflowers and Their Superior Electrocatalytic Activity for the Oxygen Reduction Reaction and Remarkable Methanol-Tolerant Ability in Acid Media. *J. Phys. Chem. C* **2013**, *117* (19), 9826−9834.

(10) Zhu, Z.; Zhai, Y.; Zhu, C.; Wang, Z.; Dong, S. Bimetallic Alloy Nanowires and Nanosponges: A Comparative Study of Peroxidase Mimetics and as Enhanced Catalysts for Oxygen Reduction Reaction. *Electrochem. Commun.* **2013**, *36*, 22−25.

(11) Liu, H.; Ye, F.; Yao, Q.; Cao, H.; Xie, J.; Lee, J. Y.; Yang, J. Stellated Ag-Pt Bimetallic Nanoparticles: An Effective Platform for Catalytic Activity Tuning. *Sci. Rep.* **2014**, *4*, 3969.

(12) Nie, M.; Zeng, Z. J.; He, B.; Li, Q.; Liu, X. W.; Zheng, C. S. Tungsten Carbide Promoted Au−Pd−Pt as Methanol Tolerant Electrocatalysts for Oxygen Reduction Reaction. *Mater. Res. Innovations* **2013**, *18* (4), 255−258.

(13) Callejas-Tovar, R.; Balbuena, P. B. Effect of Subsurface Vacancies on Oxygen Reduction Reaction Activity of Pt-Based Alloys. *J. Phys. Chem. C* **2012**, *116* (27), 14414−14422.

(14) Kattel, S.; Duan, Z.; Wang, G. Density Functional Theory Study of an Oxygen Reduction Reaction on a Pt_3Ti Alloy Electrocatalyst. *J. Phys. Chem. C* **2013**, *117* (14), 7107−7113.

(15) Zhu, H.; Zhang, S.; Guo, S.; Su, D.; Sun, S. Synthetic Control of FePtM Nanorods (M = Cu, Ni) To Enhance the Oxygen Reduction Reaction. *J. Am. Chem. Soc.* **2013**, *135* (19), 7130−7133.
(16) Yue, Q.; Zhang, K.; Chen, X.; Wang, L.; Zhao, J.; Liu, J.; Jia, J. Generation of OH Radicals in Oxygen Reduction Reaction at Pt-Co Nanoparticles Supported on Graphene in Alkaline Solutions. *Chem. Commun.* **2010**, *46* (19), 3369−3371.
(17) Mohanraju, K.; Cindrella, L. Impact of Alloying and Lattice Strain on ORR Activity of Pt and Pd based Ternary Alloys with Fe and Co for Proton Exchange Membrane Fuel Cell Applications. *RSC Adv.* **2014**, *4* (23), 11939−11947.
(18) Guo, S.; Sun, S. FePt Nanoparticles Assembled on Graphene as Enhanced Catalyst for Oxygen Reduction Reaction. *J. Am. Chem. Soc.* **2012**, *134* (5), 2492−2495.
(19) Guo, S.; Zhang, S.; Su, D.; Sun, S. Seed-Mediated Synthesis of Core/Shell FePtM/FePt (M = Pd, Au) Nanowires and Their Electrocatalysis for Oxygen Reduction Reaction. *J. Am. Chem. Soc.* **2013**, *135* (37), 13879−13884.
(20) Zhang, S.; Guo, S.; Zhu, H.; Su, D.; Sun, S. Structure-Induced Enhancement in Electrooxidation of Trimetallic FePtAu Nanoparticles. *J. Am. Chem. Soc.* **2012**, *134* (11), 5060−5063.
(21) Xu, C.; Li, Q.; Liu, Y.; Wang, J.; Geng, H. Hierarchical Nanoporous PtFe Alloy with Multimodal Size Distributions and Its Catalytic Performance toward Methanol Electrooxidation. *Langmuir* **2012**, *28* (3), 1886−1892.
(22) Zhu, C.; Guo, S.; Dong, S. Rapid, General Synthesis of PdPt Bimetallic Alloy Nanosponges and Their Enhanced Catalytic Performance for Ethanol/Methanol Electrooxidation in an Alkaline Medium. *Chem.—Eur. J.* **2013**, *19* (3), 1104−1111.
(23) Huang, X.; Zhu, E.; Chen, Y.; Li, Y.; Chiu, C.-Y.; Xu, Y.; Lin, Z.; Duan, X.; Huang, Y. A Facile Strategy to Pt_3Ni Nanocrystals with Highly Porous Features as an Enhanced Oxygen Reduction Reaction Catalyst. *Adv. Mater.* **2013**, *25* (21), 2974−2979.
(24) Stamenkovic, V. R.; Fowler, B.; Mun, B. S.; Wang, G.; Ross, P. N.; Lucas, C. A.; Marković, N. M. Improved Oxygen Reduction Activity on $Pt_3Ni(111)$ via Increased Surface Site Availability. *Science* **2007**, *315* (5811), 493−497.
(25) Duchesne, P. N.; Chen, G.; Zheng, N.; Zhang, P. Local Structure, Electronic Behavior, and Electrocatalytic Reactivity of CO-Reduced Platinum−Iron Oxide Nanoparticles. *J. Phys. Chem. C* **2013**, *117* (49), 26324−26333.